Energy & Environmental Science

Cite this: *Energy Environ. Sci.*, 2011, **4**, 1465

www.rsc.org/ees

PAPER

Synthesis of transparent mesoporous tungsten trioxide films with enhanced photoelectrochemical response: application to unassisted solar water splitting†

Jung Kyu Kim,‡[a] Kahee Shin,‡[a] Sung M. Cho,[a] Tae-Woo Lee[b] and Jong Hyeok Park*[a]

Received 23rd September 2010, Accepted 4th February 2011
DOI: 10.1039/c0ee00469c

Tungsten trioxide (WO_3) films with a mesoporous morphology, high transparency, and monoclinic phase crystallinity were prepared using polyethyleneglycol (PEG) as a surfactant and their photoelectrochemical properties were measured. By controlling the weight ratio of the tungsten precursor to PEG, a sphere-like WO_3 nanoparticle film with high transparency can be synthesized. The photocurrent responses of the films under 1 sun solar light illumination were measured. Due to the high transparency of the WO_3 photoanode, it is possible to fabricate a tandem cell composed of a WO_3/Pt bipolar electrode connected with a dye-sensitized solar cell. Unassisted water splitting from the tandem cell was demonstrated but the maximum current density was exhibited at around +0.4 V (*vs.* Pt).

Introduction

As global warming due to carbon dioxide (CO_2) emissions becomes increasingly important, worldwide research has been focused on developing a clean and renewable energy source. Since Fujishima and Honda reported photoelectrochemical water splitting using a titanium dioxide (TiO_2) semiconductor photoanode in 1972,[1] solar hydrogen generation by water splitting has been considered one of the best ways to convert a naturally abundant and benign substance into an energy source.[2] The amounts of usable solar energy and water are unlimited, and there are no pollutants generated as byproducts such as CO_2. However, solar water splitting with a photoelectrochemical cell has some problems to overcome for commercialization due to its low efficiency. Therefore, intensive research on solar hydrogen generation has focused on achieving a higher efficiency and better performance by using materials with a relatively smaller band gap than TiO_2 to expand visible light absorption.

Several research groups reported the use of other oxide materials such as tungsten trioxide (WO_3)[3–6] and iron oxide (Fe_2O_3).[7] Moreover, efforts to enhance the efficiency by controlling the nanostructure of the photoanode have been conducted to maximize the contact area between the electrode and electrolyte and to optimize the electron transport pathways. In previous studies, many types of nanostructured photoanodes were used for water splitting including nanotube arrays,[8–11] nanowire,[12,13] nanosheet,[14] and nanorod arrays.[15]

To use a metal oxide-based photoanode in an unassisted solar water splitting system, the valence and conduction bands in the semiconductor material should be more positive than the oxidation potential of water and more negative than the reduction potential of protons, respectively. Unfortunately, the energy level of the conduction band of oxide materials such as WO_3 or Fe_2O_3 cannot contain the sufficient reduction potential of

[a]*School of Chemical Engineering, and SKKU Advanced Institute of Nanotechnology (SAINT), Sungkyunkwan University, Suwon, 440-746, Korea. E-mail: lutts@skku.edu*
[b]*Department of Materials Science and Engineering, Pohang University of Science and Technology, San 31, Hyoja-dong, Nam-gu, Pohang, Gyeongbuk 790-784, Korea*

† Electronic supplementary information (ESI) available: UV-vis data, photocurrent data and hydrogen evolution data. See DOI: 10.1039/c0ee00469c

‡ Jung Kyu Kim and Kahee Shin contributed to this work equally.

Broader context

Tungsten trioxide (WO_3) films with a mesoporous morphology, high transparency, and monoclinic phase crystallinity were prepared using polyethyleneglycol (PEG) as a surfactant and their photoelectrochemical properties were measured. By controlling the weight ratio of the tungsten precursor to PEG, a sphere-like WO_3 nanoparticle film with high transparency can be synthesized. The photocurrent responses of the films under 1 sun solar light illumination were measured. Due to the high transparency of the WO_3 photoanode, it is possible to fabricate a tandem cell composed of a WO_3/Pt bipolar electrode connected with a dye-sensitized solar cell. Unassisted water splitting from the tandem cell was demonstrated but the maximum current density was exhibited at around +0.4 V (*vs.* Pt).

protons. Thus, it is necessary to apply an external bias to generate hydrogen efficiently.[16] To realize an unassisted water splitting system, the metal oxides should be combined with other energy generating devices such as a dye-sensitized solar cell, which is usually referred to as a tandem cell.[17] To use a metal oxide as a photoanode for the tandem cell, it should exhibit not only a high photocurrent density but also a high transparency because long wavelength solar light should be harvested by dye molecules in the dye-sensitized solar cell located at the backside of the photoanode.

In this paper, we report the synthesis of transparent mesoporous tungsten trioxide films prepared by a surfactant-assisted sol–gel reaction utilizing a colloidal solution of tungstic acid with poly(ethylene glycol) 300 as an organic stabilizer. The organic additive was previously reported to play a role as a template for the formation of the nanostructure in the precursor solution resulting in different nanostructures of the metal oxide.[16,18,19] We optimized the WO_3 film morphology to result in a proper transparency and high photocurrent density by controlling the composition of the precursor mixture or the film thickness by changing the number of deposition steps. Finally, we fabricated a novel photoanode/DSSC tandem cell to obtain the unassisted water splitting system.

Experimental

Synthesis of WO_3 nanostructured films

The nanostructured WO_3 films used in this study were deposited on transparent conducting glass substrates (F-doped SnO_2-coated glass, FTO). The solution used for the deposition of WO_3 was a colloidal complex consisting of peroxy-tungstic acid and poly(ethylene glycol) 300 as an organic stabilizing and structure controlling agent.[20] The peroxy-tungstate precursor was obtained by dissolving tungsten powder (Acros, 99.9%) in hydrogen peroxide (30% H_2O_2, Junsei). 9 g of W was dissolved in 10 ml of H_2O_2. Then, 25 ml of IPA (2-propanol, Junsei) was added to this solution to improve the stability and PEG 300 (poly(ethylene glycol) 300, Aldrich) was added to improve the effectiveness of the porous nanostructure.[18] It is known that the organic solvent, IPA, slows down the condensation of tungstate[21] and these compounds make complexes with tungsten oxoanions.[22] However, the prepared solution should be used within 2 days. If the solution was used after 2 days, the mesoporous WO_3 film developed serious cracks during the annealing process.

The nanostructured porous WO_3 films on the TCO were obtained by applying the following procedure: (1) dropping 20 μl of the precursor onto the FTO glass (dimension: 1.5 cm × 1.5 cm) and drying at room temperature for 20 min, (2) repeating this process (dropping and drying) two more times, and (3) annealing the as-deposited films at 550 °C for 30 min. These processes (3× dropping and drying and 3× annealing) are referred to as 1 cycle. The thermal annealing process at the high temperature was conducted to obtain monoclinic WO_3 (crystalline m-WO_3) and to improve the nano-crystallinity of the film.[23] The samples used in this study were obtained by applying 1 cycle and 3 cycles. The 1 cycle samples were prepared with weight ratios of tungsten to PEG 300 of 1 : 0, 1 : 2, 1 : 5, 1 : 10, and 1 : 30.

Characterization methods

To examine the morphology of the samples, the field emission scanning electron microscopy (FE-SEM, JSM-7000F, Japan) was used. X-Ray diffraction measurements were carried out to observe the crystalline phase with a Siemens diffractometer D500/5000 in Bragg-Bretano geometry under Cu K radiation. Also, the optical properties of the samples were investigated using a UV-vis spectrophotometer (UV-2401 PC, Shimadzu).

Photoelectrochemical measurements

The electrochemical responses were investigated using a 3-electrode configuration with Pt as a counter electrode and Ag/AgCl as a reference electrode (CH Instruments, CHI 660) in a 1 M sulfuric acid solution as an electrolyte. The linear sweep voltammetry technique was used at a scan rate of 10 mV s^{-1}. The working electrode was illuminated with a 150 W xenon lamp-based solar simulator (PECCELL, Yokohama, Japan, PEC-L01: 100 mW cm^{-2}). The light intensity was calibrated using a silicon reference cell (Fraunhofer ISE, Certificate No. C-ISE269) and the measured light irradiance was 100 mW cm^{-2}.

Tandem cell fabrication

A dye-sensitized solar cell (DSSC) was employed as a tandem cell in a photovoltaic system. An anatase single-layered TiO_2 mesoporous film was used as a photoanode of the DSSC. A 10 μm thick TiO_2 nanoparticle film was deposited on a pretreated FTO glass substrate by applying UV with a $TiCl_4$ solution. After annealing at 550 °C for 30 min, the nanocrystalline TiO_2 electrode was immersed in a N719 dye solution for 18 hours to allow chemisorption of the dye molecules. The counter electrode of the DSSC was prepared by spincoating a FTO glass substrate with a H_2PtCl_6 solution and heating it at 550 °C for 30 min. A porous WO_3 film was coated on the backside of the counter electrode of the DSSC to produce a bipolar WO_3/Pt electrode by using the precursor solution (W : PEG = 1 : 10) in 1 cycle. Because FTO was covered on each side of the glass substrate, the generated electrons from the WO_3 electrode can be easily transferred to the Pt electrode.

Results and discussion

Generally, the WO_3 film morphology was strongly dependent on the addition of the organic additive. The morphologies of the WO_3 films prepared from various precursor solutions with different amounts of PEG were observed by SEM, as shown in Fig. 1.

Fig. 1a shows an SEM image of the WO_3 film made using a pure tungstic acid precursor solution without PEG. Agglomerated WO_3 particles with nonuniform shapes are observed in the top-view image. The WO_3 film prepared from the solution with W : PEG = 1 : 1 (by wt) had a flat film structure which was not a porous structure, as shown in Fig. 1b. Instead, there were several hundred nanometre-sized embedded ball-like particles on the film surface. This may be considered as the starting point for the formation of mesoporous structures. Similarly, the WO_3 film prepared from the solution with W : PEG = 1 : 2 (by wt) had a flat film structure with several hundred nanometre-sized

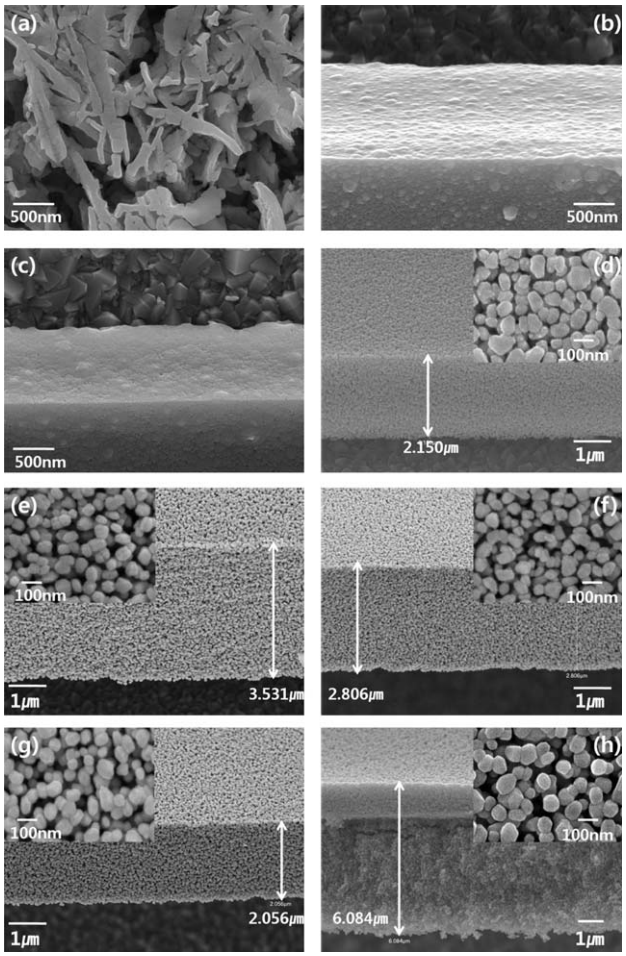

Fig. 1 SEM images of 1 cycle-deposited WO_3 films on FTO glass made using tungstic acid precursor solutions with W : PEG 300 = (a) 1 : 0, (b) 1 : 1, (c) 1 : 2, (d) 1 : 5, (e) 1 : 10, (f) 1 : 20, and (g) 1 : 30. (h) SEM image of a 3-cycle deposited WO_3 film prepared from the tungstic acid precursor solution with W : PEG 300 = 1 : 10.

embedded ball-like particles on the film surface, as shown in Fig. 1c. However, there are many narrow cracks between the embedded ball-like particles on the surface of this film. Fig. 1d shows an SEM image of the mesoporous WO_3 film produced using tungstic acid and the PEG complex precursor with a W : PEG weight ratio of 1 : 5. This film consisted of assembled WO_3 nanobeads with diameters of ~100 nm and the thickness of the film was 2.1 μm. Considering the characteristics and properties of the photoelectrode which requires a large interface between the electrolyte and the films, this porous structure is important for increasing the efficiency of water splitting since the generated electron and hole pairs will only have a small chance to recombine before participating in the electrochemical reaction. Fig. 1e shows an SEM image of the porous WO_3 film obtained from the precursor solution with W : PEG = 1 : 10 (by wt). The morphology of this film is similar to the previous film (Fig. 1d) but there are some important differences. In the W : PEG = 1 : 10 film, the distances from one nano-bead to another are greater and the shape of the beads is more spherical than in the W : PEG = 1 : 5 film. The film shown in Fig. 1f (W : PEG = 1 : 20) has a similar structure, morphology, and porosity to the W : PEG = 1 : 10 film. However, it had a mesoporous film thickness of 2.8 μm, which is 730 nm less than the thickness of the WO_3 film prepared with W : PEG = 1 : 10. The phenomena of thickness reduction without changes of the structure, morphology, and porosity was also observed in the WO_3 film prepared from the W : PEG = 1 : 30 precursor solution, as shown in Fig. 1g. As determined from the SEM image, the W : PEG = 1 : 30 mesoporous film exhibited a thickness of 2.1 μm. We can conclude that the thickness of the mesoporous WO_3 film as well as the film morphology is controllable by the W : organic stabilizer weight ratio in the precursor solution. Fig. 1h shows the morphology of the WO_3 film obtained from three cycles of deposition of the precursor solution with W : PEG = 1 : 10 (by wt). The morphology of this film is similar to the film prepared from the same precursor solution but the size of the nano-beads is a little larger than those observed in Fig. 1e. Moreover, the thickness of this film was about 6.1 μm.

The X-ray diffraction (XRD) patterns of the nanostructured WO_3 films shown in Fig. 2 confirm the dependency of the crystalline structure as a function of the added organic stabilizer. The films consisted of sphere-like particles (1 : 5 and 1 : 10 W : PEG ratios) indexed to (monoclinic) WO_3 in terms of the peak positions (JCPDS No. 43-1035). However, the WO_3 films obtained from precursor solutions with W : PEG ratios of 1 : 0 and 1 : 2, which did not have nanoparticulate nanostructures, had higher peaks at the 202 and 220 positions and different peak positions from the other films, which were indexed to (orthorhombic) WO_3 (JCPDS No. 20-1324). From these results, it was confirmed that the organic additive acts as a crystallinity controller, which is another important function of PEG 300. Fig. 3 shows the UV-vis absorption spectra for the series of WO_3 films. All of the samples start to absorb light between about 480 nm and 496 nm, which corresponds to a band gap of around 2.58 eV and 2.50 eV. However, the shift of the absorption edge in nanoparticle to higher energies compared to that of bulk film can be seen, indicating a widening of the energy gap caused by quantum size effects. The similar behavior is also reported by Sun *et al.*[24] Particularly, the energies of band edge increase because of the decrease in the particles size of the nanoparticles. To investigate the effect of the crystallinity of WO_3 on its band gap energy, WO_3 films with different crystalline structures were prepared from

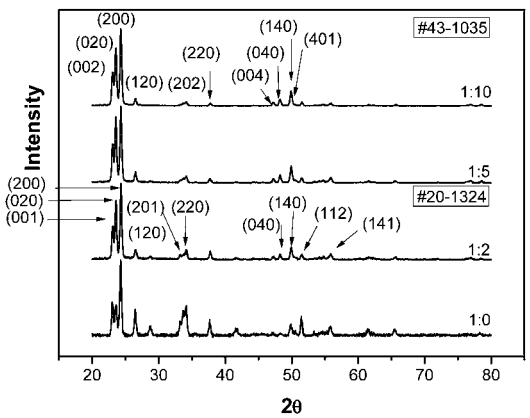

Fig. 2 X-Ray diffraction data of WO_3 films obtained by using W : PEG 300 weight ratios of 1 : 0, 1 : 2, 1 : 5, and 1 : 10.

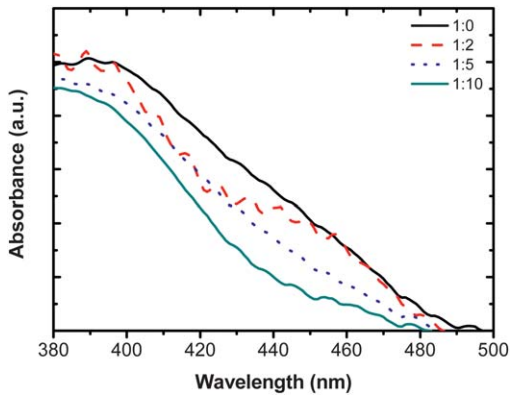

Fig. 3 UV-vis absorbance spectra of nanostructured WO_3 films obtained by using W : PEG 300 weight ratios of 1 : 0, 1 : 2, 1 : 5, and 1 : 10.

a pure tungsten precursor solution and their UV-vis absorption spectra were shown in Fig. S1†. The orthorhombic structure showed smaller band gap energy compared with that of the monoclinic structure.

Fig. 4 shows the photoelectrochemical responses of the nanostructured WO_3 films as a function of the W : PEG 300 ratio in the precursor solutions (1 : 0, 1 : 5, 1 : 10, and 1 : 30). Also, the thickness dependence was investigated by using a fixed 1 : 10 ratio of the W : PEG precursor solution. The photocurrent density increased from about 1.1 mA cm^{-2} to about 2.2 mA cm^{-2} (for the 1 : 10 precursor solution) as the concentration of PEG was increased. However, when the PEG content exceeded a certain level, the photocurrent density decreased.

As seen in Fig. 1d and f, there were no differences in the structures of the films prepared with 1 : 5 and 1 : 20 W : PEG 300 ratios. However, after sintering the nanostructured WO_3 films, the thickness of the films decreased as the concentration of PEG increased, which decreases the total number of electrons and holes to participate in the electrochemical reaction. Therefore, the 1 : 30 sample had a smaller photocurrent density than the 1 : 10 sample. Fig. S2† shows the photoelectrochemical responses of the nanostructured WO_3 films normalized by their film thickness as a function of the W : PEG 300 ratio in the precursor solutions (1 : 0, 1 5 , 1 : 10, and 1 : 30). As can be seen in Fig. 3, the shift of the absorption edge in nanoparticle to higher energies has negative effect on the photocurrent generation. However, all samples with nanostructured WO_3 represent improved photocurrent than that of non-porous WO_3 film. This means that the positive effect of increased porosity on the photocurrent is more dominant. The nanostructural morphology can increase the contact area between WO_3 and the electrolyte, resulting in decreased electron/hole recombination. The films prepared with 1 : 5 and 1 : 10 W : PEG300 ratios represent very similar *I–V* characteristics as we expected from the morphology data (Fig. 1d and e). However, further increase of PEG content reduces the photocurrent density. Even though the film morphology prepared with 1 : 20 W : PEG300 do not show significant differences compared to the films prepared with 1 : 5 or 1 : 10 ratios, it can be anticipated that the bad connection among WO_3 nanoparticles might induce poor interfacial characteristics, resulting in decreased photocurrent density. Also, we investigated the photocurrent of the thicker film produced using the 1 : 10 solution over 3 cycles. The thicker film produced a photocurrent density of about 3.7 mA cm^{-2}. Moreover, the sample demonstrated a photocurrent density of about 5.1 mA cm^{-2} after addition of 0.1 M methanol as a sacrificial reagent, which is due to the oxidation of methanol instead of water decomposition. This phenomenon can be referred to as photocurrent doubling, in which an additional electron is injected in the conduction band of the electrode during the photodecomposition of methanol.[25]

Fig. 5 shows the transmittance spectra of (a) a bare FTO glass, (b) the nanostructured WO_3 film prepared from the solution of W : PEG = 1 : 10 (by wt), (c) and the WO_3 film without organic stabilizer. The transmittance intensity of the bare substrate is about 74% and the nanostructured WO_3 film has a suitable transparency of about 58% at 730 nm, which can permit the solar absorption of dye molecules in DSSCs. Therefore, it is obvious that this nanostructural transparent WO_3 film is suitable as a photoanode in the tandem cell. However, the transmittance intensity of the WO_3 film prepared without the organic stabilizer is about 25%, which is far lower than the intensity of the nanostructural film demonstrating that it is less suitable for use as the photoanode than the nanostructural film. The three photographs displayed in Fig. 6 exhibit the transparency of the nanostructured

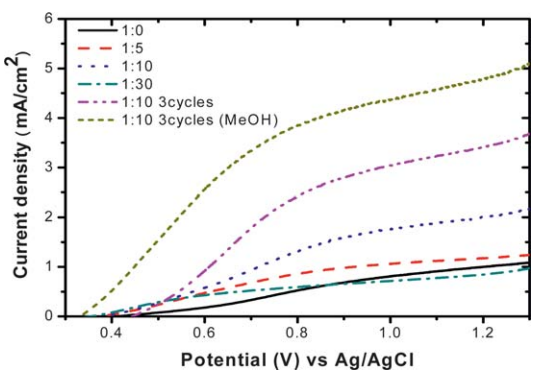

Fig. 4 Photocurrent densities of the nanostructured WO_3 films under 100 mW cm^{-2} illumination.

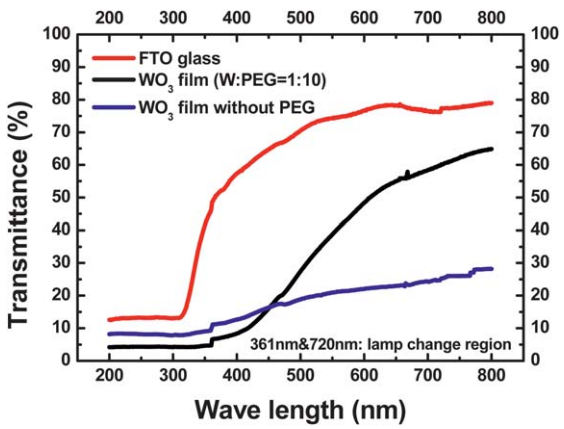

Fig. 5 Transmittance spectra of a bare FTO glass, the nanostructured WO_3 film with W : PEG 300 = 1 : 10, and the WO_3 film without PEG 300.

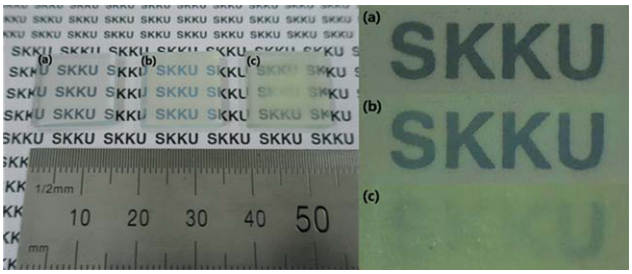

Fig. 6 Photographs of (a) a bare FTO glass, (b) the nanostructured WO_3 film with W : PEG 300 = 1 : 10, and (c) the WO_3 film without PEG 300.

WO_3 film. There are only small differences between the images of the bare FTO glass (a) and the nanostructured film (b). However, there are significant differences between the images of the nanostructured film (b) and the WO_3 film prepared without organic stabilizer (c).

A schematic diagram of the photoanode/photovoltaic tandem cell consisting of a semi-transparent WO_3 film (W : PEG = 1 : 10 (by wt), 1 cycle) in the DSSC is shown in Fig. 7a. A WO_3 nanoparticulate thin film was deposited on one side of a FTO glass substrate and the other side was covered with a platinum counter electrode for the DSSC. Once light is incident to the semi-transparent photoanode, WO_3 nanoparticles can absorb short wavelength light (~496 nm, theoretically), exciting electrons in the valence band of WO_3 to the conduction band. Then, the harvested electrons move to the right side of the FTO glass substrate toward the platinum cathode of the DSSC. The electrons are used to reduce triiodide to iodide in the DSSC electrolyte. Holes remaining in the valence band oxidize water to oxygen. Long wavelength light not absorbed by WO_3 may penetrate the photoanode, platinum-coated FTO glass, and I^-/I_3^- electrolyte to finally reach the anode of the DSSC. Then, electrons in the dye molecules on the anode are excited from the HOMO to the LUMO. The electrons move to the counter electrode through an external circuit, reducing protons in the water electrolyte to hydrogen. Note that the inner I^-/I_3^- electrolyte prevents contact with outer water electrolyte by sealing material. In this process, the DSSC can provide the additional required potential to the photoanode so that this tandem cell does not need to be applied with an external bias. In Fig. 7b, the photocurrent responses of the nanostructured WO_3 films are shown. The presented *I–V* data were obtained from a 2-electrode system. Because the counter electrode and reference electrode are Pt, the potential refers to an externally applied voltage. The solid line represents the *I–V* of the photoanode in the tandem cell and the dashed line is the result from the WO_3 photoelectrode. The onset potential of the tandem photoanode was negatively shifted by about 0.6 V, which corresponds to the V_{oc} of the DSSC used in the tandem cell. The tandem cell started to generate hydrogen at a voltage of 0.2 V negative of the 0 V bias, indicating that an additional external voltage was not needed for this tandem cell to split water. The light-limiting current was reached at a positive bias (~0.4 V) and remained almost constant with increasing bias. The zero bias point represents the maximum short-circuit photocurrent for water splitting and is the operating point for the tandem cell in the photoelectrolysis mode without an external bias. This current is a result of a combination of the voltage produced in the tandem cell and the voltage needed for water splitting at that photocurrent density.

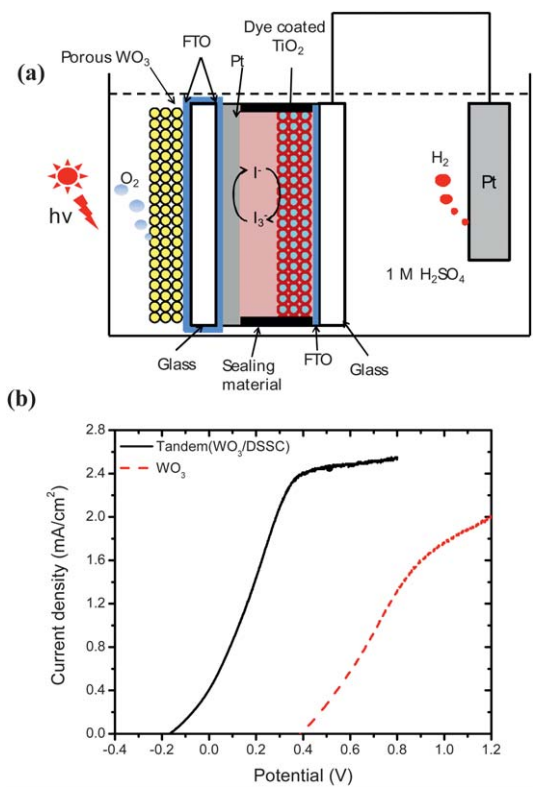

Fig. 7 (a) Schematic diagram of the photovoltaic/photoelectrochemical tandem cell with the DSSC and a WO_3 photoelectrode. (b) The *I–V* curve of the neat WO_3 film and WO_3/DSSC tandem cell under 100 mW cm^{-2} illumination.

Fig. S3† shows the hydrogen generation rates for three different cells. It was confirmed that the tandem cell only can generate hydrogen from water without an external bias. The stability of the tandem cell was observed using a two-electrode photoelectrochemical cell. The photocurrent response of the tandem cell under the illumination without external potential is shown in Fig. S4†. The current response of the tandem cell to UV-visible light illumination from a solar simulator was prompt. There is no significant decrease in the photocurrent for about 30 min representing good electrochemical stability under illumination.

Conclusions

We investigated the effects of using PEG as a surfactant on the formation of WO_3 nanoparticles and their photocurrent response for hydrogen generation. As expected, the photocurrent density was influenced by the morphology of the films. Moreover, the nanoparticulate films showed improved transmittance at UV-vis wavelengths. This behavior is very important for the fabrication of WO_3/DSSC tandem cells. We also prepared WO_3/DSSC tandem cells by using a bipolar WO_3/Pt electrode connected with a dye-coated TiO_2 photoelectrode through an iodine/triiodide electrolyte. The tandem cell successfully demonstrated the unassisted water splitting reaction. We believe that this

unique approach can stimulate the development of WO_3/DSSC tandem cells.

Acknowledgements

This research was supported by Future-based Technology Development Program (Nano Fields) through the National Research Foundation of Korea (NRF) funded by the Ministry of Education, Science and Technology (2010-0029321). This work was supported by the National Research Foundation of Korea Grant funded by the Korean Government (MEST) (NRF-2009-C1AAA001-2009-0094157, 2009-0083540). This work was also partially supported by the Hydrogen Energy R&D Center, one of the 21st Century Frontier R&D Programs, funded by the Ministry of Education, Science and Technology of Korea.

References

1 A. Fujishima and K. Honda, *Nature*, 1972, **238**, 37.
2 Z. G. Zou, J. H. Ye, K. Sayama and H. Arakawa, *Nature*, 2001, **414**, 625.
3 A. Enesca, A. Duta and J. Schoonman, *Thin Solid Films*, 2007, **515**, 6371.
4 C. Santato, M. Ulmann and J. Augustynski, *J. Phys. Chem. B*, 2001, **105**, 936.
5 B. Yang, Y. J. Zhang, E. Drabarek, P. R. F. Barnes and V. Luca, *Chem. Mater.*, 2007, **19**, 5664.
6 M. Yagi, S. Maruyama, K. Sone, K. Nagai and T. Norimatsu, *J. Solid State Chem.*, 2008, **181**, 175.
7 S. U. M. Khan and J. Akikusa, *J. Phys. Chem. B*, 1999, **103**, 7184.
8 G. K. Mor, K. Shankar, M. Paulose, O. K. Varghese and C. A. Grimes, *Nano Lett.*, 2005, **5**, 191.
9 N. K. Allam, K. Shankar and C. A. Grimes, *J. Mater. Chem.*, 2008, **18**, 2341.
10 Q. Q. Chen, D. S. Xu, Z. Y. Wu and Z. F. Liu, *Nanotechnology*, 2008, **19**, 5.
11 E. Y. Kim, J. H. Park and G. Y. Han, *J. Power Sources*, 2008, **184**, 284.
12 S. U. M. Khan and T. Sultana, *Sol. Energy Mater. Sol. Cells*, 2003, **76**, 211.
13 M. Kitano, R. Mitsui, D. R. Eddy, Z. M. A. El-Bahy, M. Matsuoka, M. Ueshima and M. Anpo, *Catal. Lett.*, 2007, **119**, 217.
14 I. Cesar, A. Kay, J. A. G. Martinez and M. Gratzel, *J. Am. Chem. Soc.*, 2006, **128**, 4582.
15 A. Wolcott, W. A. Smith, T. R. Kuykendall, Y. P. Zhao and J. Z. Zhang, *Small*, 2009, **5**, 104.
16 B. D. Alexander, P. J. Kulesza, L. Rutkowska, R. Solarska and J. Augustynski, *J. Mater. Chem.*, 2008, **18**, 2298.
17 M. Gratzel, *Nature*, 2001, **414**, 338.
18 C. Santato, M. Ulmann and J. Augustynski, *Adv. Mater.*, 2001, **13**, 511.
19 L. Meda, G. Tozzola, A. Tacca, G. Marra, S. Caramori, V. Cristino and C. A. Bignozzi, *Sol. Energy Mater. Sol. Cells*, 2010, **94**, 788.
20 R. Solarska, C. Santato, C. Jorand-Sartoretti, M. Ulmann and J. Augustynski, *J. Appl. Electrochem.*, 2005, **35**, 715.
21 L. Jean and L. Jean, *Can. J. Chem.*, 1977, **55**, 3758.
22 E. Richardson, *J. Inorg. Nucl. Chem.*, 1959, **12**, 79.
23 C. Santato, M. Odziemkowski, M. Ulmann and J. Augustynski, *J. Am. Chem. Soc.*, 2001, **123**, 10639.
24 W. Sun, L. Xu, Y. Chu and W. Shi, *J. Colloid Interface Sci.*, 2003, **266**, 99.
25 S. R. Morrison and T. Freund, *J. Chem. Phys.*, 1967, **47**, 1543.

